European Journal of Mechanics B/Fluids 29 (2010) 132–142

Contents lists available at ScienceDirect

European Journal of Mechanics B/Fluids

journal homepage: www.elsevier.com/locate/ejmflu

Generation of two-dimensional steep water waves on finite depth with and without wind

J. Chambarel*, C. Kharif, O. Kimmoun

Institut de Recherche sur les Phénomènes Hors Equilibre, IRPHE – UMR 6594, Technopôle de Château-Gombert 49, rue Joliot Curie, B.P. 146, 13384 Marseille Cedex 13, France

ARTICLE INFO

Article history:
Received 4 August 2009
Received in revised form
12 October 2009
Accepted 15 December 2009
Available online 29 December 2009

Keywords:
Dispersive focusing
Steep wave train
Breaking wave
Shallow water
Wind
Jeffreys sheltering mechanism

ABSTRACT

This paper reports on a series of numerical simulations designed to investigate the action of wind on steep waves and breaking waves generated through the mechanism of dispersive focusing on finite depth. The dynamics of the wave packet propagating without wind at the free surface are compared to the dynamics of the packet propagating in the presence of wind. Wind is introduced in the numerical wave tank by means of a pressure term, corresponding to the modified Jeffreys' sheltering mechanism. The wind blowing over a strongly modulated wave group due to the dispersive focusing of an initial long wave packet increases the duration and maximal amplitude of the steep wave event. These results are coherent with those obtained within the framework of deep water. However, steep wave events are less unstable to wind perturbation in shallow water than in deep water.

Furthermore, a comparison between experimental and numerical wave breaking is presented in the absence of wind. The numerical simulations show that the wind speeds up the wave breaking and amplifies slightly the wave height.

The wall pressure during the runup of the steep wave event on a vertical wall is also investigated and a comparison between experimental and numerical results is provided.

1. Introduction

Extreme wave events are due to the focusing of wave energy into a small area. The main physical mechanisms which may produce extreme wave events are described and discussed in detail in Kharif et al., 2009 [1]. Extreme wave occurrence on currents is a well-understood problem that can explain the formation of rogue waves when wind waves or swells are propagating against a current. Geometrical or spatial focusing may result in large-amplitude waves. The spatio-temporal wave focusing due to the dispersive nature of water waves is a classic mechanism yielding wave energy concentration in a small area. Nonlinear uniform wave trains suffer an instability known as the Benjamin–Feir instability, which produces growing modulations of the envelope that evolve into short groups of steep waves. A uniform wave train under modulational instability transforms into a system of envelope that may collide to give rise to huge wave events. Most of the studies have considered the extreme wave occurrence without including the direct effect of the wind on their dynamics. To our knowledge, there are few published results about this coupling. Among the recent papers on wind forcing on large-amplitude deep water waves, one can cite Banner and Song, 2002 [2], Touboul et al., 2006 [3] and Kharif et al., 2008 [4]. Ma and Yan, 2008 [5] presented preliminary simulations of wind effects on two- and three-dimensional freak waves on finite depth. Recently, Yan and Ma, 2009 [6] investigated numerically wind effects on two-dimensional breaking solitary waves on a sloping beach. Within the framework of extreme wave events due to the spatio-temporal focusing and Benjamin–Feir instability, Touboul et al., 2006 [3] and Kharif et al., 2008 [4] have shown experimentally and numerically that wind sustains steep waves which then evolve into breaking waves. More specifically, wind increases both the amplitude and lifetime of steep wave events. Wind effect plays a significant role in the persistence of extreme wave events. Until now there has been no investigation on wind effect on the formation of extreme wave events in shallow water apart from the papers by Chambarel et al., [7] and Yan and Ma, 2009 [6]. Note that Chambarel et al. [7] considered only one kind of focusing by using an inverse method and extended previous results of Touboul et al., 2006 [3] and Kharif et al., 2008 [4] obtained in deep water to extreme wave events with wind forcing in shallow water. Within the framework of one-dimensional propagation it is well known that the Benjamin–Feir instability stabilizes when kh becomes less than 1.363, where k and h are the wavenumber and depth respectively. Hence we shall use two different kinds of spatio-temporal wave focusing (or dispersive

* Corresponding author. Tel.: +33 4 96 13 98 61.
E-mail address: chambarel@irphe.univ-mrs.fr (J. Chambarel).

0997-7546/$ – see front matter © 2009 Elsevier Masson SAS. All rights reserved.
doi:10.1016/j.euromechflu.2009.12.002

focusing) for generating extreme wave events. One of the purposes of the present study is to extend and complete the paper by Chambarel et al. [7]. Note that rogue occurrence in shallow water is discussed in Kharif et al., 2009 [1] too, but without considering wind/wave coupling.

The second problem considered is breaking wave impact on a vertical wall. Coastal structures such as vertical breakwaters or sea walls have been damaged when subjected to steep storm waves (Oumeraci, 1994 [8]). Therefore, accurate prediction of the most severe wave loading is crucial to the design of many types of coastal structures and it is well known that when a wave breaks directly onto a vertical wall, impact pressures are produced which can be extremely large in comparison to the pressures exerted by non-breaking waves. The fundamental role of the extreme impact pressures that are impulsively exerted on sea walls has been underlined by both experimental (e.g. Chan and Melville, 1988 [9]; Kirkgneöz, 1990 [10], Kirkgzö, 1991 [11]; Hattori et al., 1994 [12]; Bullock et al., 2007 [13]) and theoretical (e.g. Cooker and Peregri, 1992 [14]; Peregrine, 2003 [15]) studies. In addition, numerous numerical models based on potential theory have been developed to provide a reliable tool for the estimation of wave shape and impact pressure (e.g. Cooker and Peregrine, 1990 [16]; Zhang et al., 1996 [17]).

In Section 2 the mathematical statement of the water wave problem is presented as well as the numerical method. Section 3 reports on two different ways used to generate steep water wave groups in finite depth. The wind modelling based on a modified sheltering mechanism is described in Section 4. Results of numerical simulations and validations are presented for both steep non-breaking waves and breaking waves in Section 5. In this section the pressure and wall force exerted by a breaking wave is computed numerically and compared with experimental data.

2. Mathematical formulation and numerical method

2.1. Basic equations

The problem is solved by assuming that the fluid is inviscid, incompressible, and the motion irrotational. Hence the velocity field is given by $\mathbf{u} = \nabla\phi$ where the velocity potential $\phi(x, z, t)$ satisfies the Laplace's equation.

$$\Delta\phi = 0 \quad \text{for} \quad -h < z < \eta(x, t) \tag{1}$$

where Δ is the Laplacian. The horizontal and vertical coordinates are x and z respectively whereas t is time. The still-water level lies at $z = 0$, and the horizontal impermeable bed lies at $z = -h$.

The Laplace equation (1) is solved within a domain bounded by the water surface and solid boundaries of the numerical tank. The boundary conditions are defined below.

The impermeability condition writes

$$\nabla\phi\cdot n = v\cdot n, \quad \text{on} \quad \partial\Omega_S, \tag{2}$$

where $\partial\Omega_S$ corresponds to solid boundaries, $\boldsymbol{v}$ is the velocity of the solid boundaries, set equal to zero on the horizontal bottom and downstream wall of the wave tank and equal to the velocity of the piston or flap at any point of the wavemaker, and $\boldsymbol{n}$ is the unit normal vector to the boundaries.

A Lagrangian description of the water surface is used

$$\frac{D\eta}{Dt} = \frac{\partial\phi}{\partial z}, \tag{3}$$

$$\frac{Dx}{Dt} = \frac{\partial\phi}{\partial x}, \tag{4}$$

where $D/Dt = \partial/\partial t + \nabla\phi\cdot\nabla$, $\nabla = (\partial/\partial x,\ \partial/\partial z)$ is the gradient operator.

The dynamic boundary condition states that the pressure at the surface is equal to the atmospheric pressure p_a

$$\frac{D\phi}{Dt} = \frac{1}{2}(\nabla\phi)^2 - g\eta + \frac{\sigma}{R} - 2\nu\frac{\partial^2\phi}{\partial z^2} - \frac{p_a}{\rho_w} \quad \text{on } z = \eta(x,t), \tag{5}$$

where σ is the surface tension coefficient, R the local curvature at the free surface, ν the viscosity coefficient, g is the acceleration due to gravity and ρ_w is the water density. The term $2\nu\partial^2\phi/\partial z^2$ is similar to the dissipative term used by Ruvinsky et al. (1991) [18].

2.2. Boundary integral equation method

The system to solve is equations (1)–(5) with the boundary conditions prescribed by equation (2). A Boundary Integral Equation Method (BIEM) is used to solve this system of equations with a mixed Euler Lagrange (MEL) time marching scheme. For more details about this numerical method see the paper by Touboul et al. [3].

The Green's second identity is used to solve Laplace's equation for the velocity potential

$$c(Q)\phi(Q) = \int_{\partial\Omega} \phi(P)\frac{\partial G}{\partial n}(P,Q)\mathrm{d}l - \int_{\partial\Omega} \frac{\partial\phi}{\partial n}(P)G(P,Q)\mathrm{d}l, \tag{6}$$

where G is the free space Green's function. The fluid domain boundary $\partial\Omega$ is $\partial\Omega_F \bigcup \partial\Omega_S$, the union of the free surface $\partial\Omega_F$ and solid boundaries $\partial\Omega_S$. The unit normal vector $\boldsymbol{n}$ points outside the fluid domain. The unknowns are $\partial\phi/\partial n$ on $\partial\Omega_F$ and ϕ on $\partial\Omega_S$. Let P, Q and $c(Q)$ denote two points of the domain and the angle between two consecutive panels respectively. The angle $c(Q)$ is defined as follows

$$c(Q) = \begin{cases} 0 & \text{if } Q \text{ is outside the fluid domain,} \\ \alpha & \text{if } Q \text{ is on the boundary,} \\ -2\pi & \text{if } Q \text{ is inside the fluid domain,} \end{cases} \tag{7}$$

where α is the inner angle relative to the fluid domain at point Q along the boundary.

Time stepping is performed using a fourth order Runge & Kutta scheme, with a constant time step.

3. Generation of steep water waves

In this section, two ways for producing steep wave events in finite depth are presented. They are both based on the dispersive nature of water waves. In the first case the steep wave events are obtained by using a numerical wave tank equipped with a piston-like wavemaker whereas in the second an inverse method is utilized to define an initial profile evolving to large waves.

3.1. Dispersive focusing

Geometrical or spatial focusing may result in large amplitude and steep waves. The spatio-temporal wave focusing due to the dispersive nature of water waves is a classic mechanism yielding wave energy concentration in a small area. Hence, we shall use the spatio-temporal wave focusing (or dispersive focusing) for generating steep wave events. Note that it is easier to generate a steep wave event through this mechanism in deep water than in shallow water. Extreme wave events due to spatio-temporal focusing phenomenon can be described as follows. In the case of dispersive wave propagation, if short wave groups are located ahead of longer wave trains, one observes that long waves will catch up the shorter

because they have a larger group velocity. A large-amplitude wave can occur at some fixed time because of superposition of all the waves merging at a given location (the focus point). Afterwards, the longer waves will be in front of the shorter waves, and the amplitude of the wave train will decrease.

A linear approach of the problem would lead to consider sea surface as a superposition of linear waves of frequencies $\omega(x, t)$. Following Whitham (1974) [19], Ostrovsky and Potapov (1999) [20] and Brown (2001) [21], the spatio-temporal evolution of these components is governing by the following hyperbolic equation:

$$\frac{\partial \omega}{\partial t} + C_g \frac{\partial \omega}{\partial x} = 0, \tag{8}$$

and hence

$$\frac{\mathrm{d}\omega}{\mathrm{d}t} = 0, \tag{9}$$

where $\mathrm{d}/\mathrm{d}t = \partial/\partial t + C_g \partial/\partial x$.

Equation (9) is true along the characteristic lines defined by $dx/dt = C_g(\omega)$ where $C_g(\omega)$ is the group velocity. This equation means that the frequency is constant along the characteristics. Finally we can describe the dispersive focusing phenomenon in the (x, t)-plane as shown in Fig. 1. A wave train is generated at $x = 0$ during $t = T$ and focus at $x = X_f$ and $t = T_f$. The straight lines correspond to different values of the wave group velocity. The question is: In what way should be modulated the initial wave train for all the characteristics originated from a given temporal interval $[0, T]$ to converge at one point $x = X_f$ at $t = T_f$? This point defines the space and time of the focusing. What is the frequency to impose to the wavemaker located at $x = 0$?

This method called inverse Fourier transform is classical in deep water (see Kharif et al. (2008) [4]), but in shallow water we cannot derive the time dependence of the frequency explicitly.

We can express the wave group velocity as a function of T_f and X_f

$$C_g = \frac{X_f}{T_f - t}, \tag{10}$$

where t is the time. Then we use the linear dispersion relation for gravity waves

$$\omega^2 = gk \tanh(kh), \tag{11}$$

to write

$$C_g = \frac{\mathrm{d}\omega}{\mathrm{d}k} = \frac{\omega}{k}\left[1 + \frac{2\,kh}{\sinh(2\,kh)}\right], \tag{12}$$

where k is the wavenumber and h the water depth. So

$$\frac{X_f}{T_f - t} = \frac{\omega}{k}\left[1 + \frac{2kh}{\sinh(2kh)}\right]. \tag{13}$$

Now we obtain a first expression of ω as a function of time

$$\omega = 2k\frac{X_f}{T_f - t}\Big/\left(1 + \frac{2\,kh}{\sinh(2\,kh)}\right). \tag{14}$$

But in this expression, k is also a function of time. So if k is known at each time step, ω may be calculated too. Using the linear dispersion relation, we can incorporate the expression of ω into equation (11).

$$k = \frac{g}{4}\left(\frac{T_f - t}{X_f}\right)^2 \tanh(kh)\left[1 + \frac{2kh}{\sinh(2kh)}\right]^2 = f(k). \tag{15}$$

The next step is to solve equation (15) by using the fixed-point method at each time step as shown in Fig. 2. Now using equation (14) the frequency ω may be known at each time. Futhermore, this method allows us to check if the value of the parameter kh, at every time step, satisfies the shallow water condition ($kh \lesssim 1$). The signal imposed to the displacement of the piston-like wavemaker in the numerical wave tank is $s(t) = A\sin(\omega(t).t)$.

3.2. Korteweg de Vries equation and inverse method

The Korteweg de Vries equation is an approximate equation which may be derived from the fully nonlinear system of equations by using a multiple scale method. The dependent variables η and ϕ are expanded as a power series of a/h with $(kh)^2 = \mathcal{O}(a/h)$, where a is a measure of the wave amplitude and k the wavenumber. The KdV equation which describes the leading-order contribution to the surface wave is

$$\frac{\partial \eta}{\partial t} + c_0\left(1 + \frac{3\eta}{2h}\right)\frac{\partial \eta}{\partial t} + \frac{c_0 h^2}{6}\frac{\partial^3 \eta}{\partial x^3} = 0, \tag{16}$$

where $c_0 = \sqrt{gh}$. Note that equation (16) holds for gravity waves only. This universal equation which describes the spatio-temporal evolution of weakly nonlinear and weakly dispersive waves is

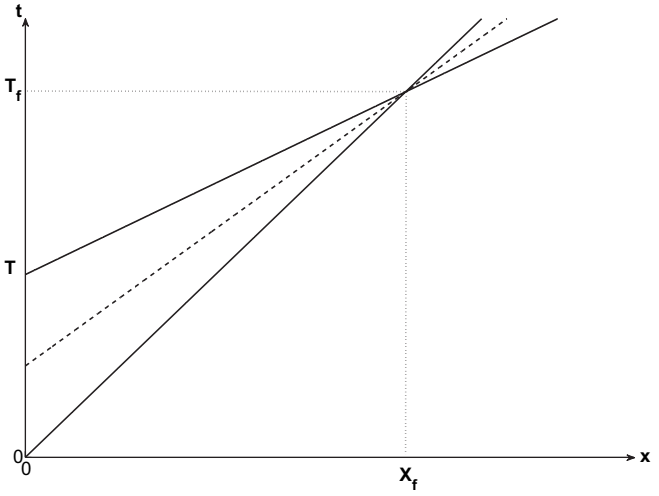

Fig. 1. Description of the dispersive focusing phenomenon in the (x, t)-plane. Characteristic lines defined by $\mathrm{d}x/\mathrm{d}t = C_g(\omega)$.

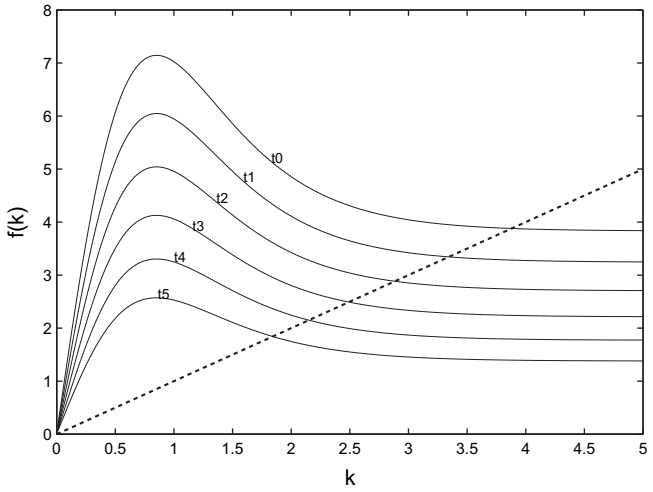

Fig. 2. Solution of equation (15) $k = f(k)$ using the fixed point method.

invariant under the transformation $x \to -x$, $t \to -t$. Hence, we can choose the expected steep wave event as the initial condition for equation (16) and calculate $\eta(x, t)$ for any time T. Due to invariance of equation (4) by reversal of abscissa, the initial condition $\eta(x, T)$ evolves to the expected steep wave event. Pelinovsky et al. [22] used this inverse method with KdV equation to study the rogue wave formation in shallow water. Following Pelinovsky et al. [22] we choose as initial condition representing the expected steep wave event the following Gaussian impulse.

$$\eta(x, 0) = A \exp\left(-K^2 x^2\right), \tag{17}$$

where A is the amplitude and K^{-1} is the initial width of the wave.

The evolution of this initial condition for equation (16) is given in Fig. 3. A pseudo-spectral method is used to compute numerically the surface elevation at different times (Fornberg (1998) [23]). At time T, a soliton is formed ahead of dispersive wave train. As expected, the soliton with the modulated wave train ahead turns into the Gaussian impulse under the inverse transformation.

The profile $\eta(x, T)$ obtained from the KdV equation with the corresponding potential $\phi(x, T)$ is then used as initial condition for numerical simulations of the fully nonlinear equation (see Fig. 4). The potential is obtained integrating the linear dynamic condition $\partial\varphi/\partial t = -g\eta$.

The dispersive wave focusing method which is linear is applicable for any value of the depth and corresponds to a boundary value problem (when a wavemaker is used for generating steep wave events). Hence this method is more appropriate than the inverse Korteweg de Vries method for comparison with experimental data.

The inverse KdV method which is weakly nonlinear is restricted to shallow water problem (i.e. small values of kh) and corresponds to initial value problems.

The choice between the two methods will depend upon the conditions under which the problem is considered.

4. Wind modelling

Within the framework of deep water, Kharif et al. [4] demonstrated experimentally for a wind velocity $U = 4$ m s that steep wave events occurring in water wave groups are accompanied by air flow separation. Furthermore, it was suggested that a significant wind effect takes place when the steep wave event occurs. The focusing stage was almost independent of the wind velocity. Deviations were observed only in the vicinity of the

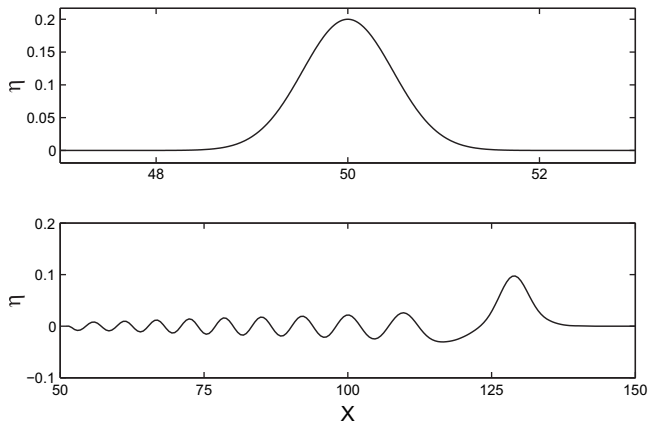

Fig. 3. Evolution of an initial Gaussian impulse (top) into soliton and dispersive wave train (bottom) within the framework of the KdV equation (η and x are given in m).

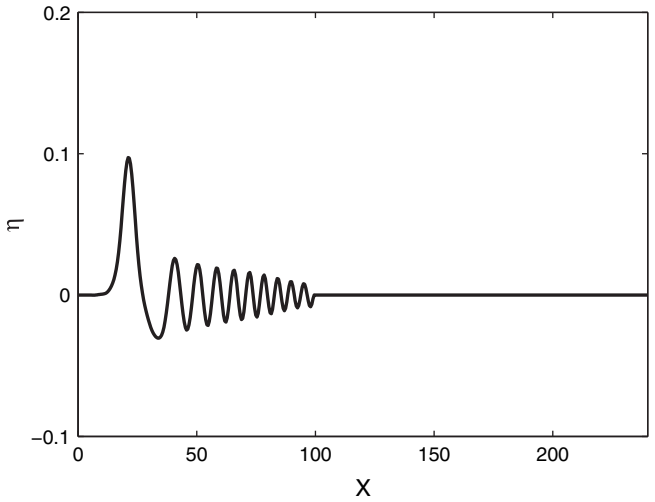

Fig. 4. Initial surface elevation from KdV equation (16) for equations (1)–(5), (η and x are given in m).

focus point where the waves become steep. This observation reinforced the idea that separation of the air flow in the lee of the wave crests is responsible for the growth and persistence of steep waves. The Jeffreys' sheltering mechanism which was introduced by Jeffreys [24] can be modified and used as wind modelling. Since air flow separation occurs only over steep waves, the Jeffreys' sheltering mechanism has to be applied locally in time and space and not permanently over the whole wave field. It is well known that this mechanism cannot be applied continuously over water waves. It is only working when air-flow separation occurs over steep waves (Banner and Melville [25], Kawai [26]). Note that the Jeffreys' sheltering mechanism is a relevant mechanism for shallow water where the waves are generally steeper than in deep water.

Following Jeffreys [24], the pressure at the interface $z = \eta(x, t)$ is related to the local wave slope according to the following expression.

$$p_a = \rho_a s (U - c)^2 \frac{\partial \eta}{\partial x}, \tag{18}$$

where the constant, s is called the sheltering coefficient, U is the wind speed, c is the wave phase velocity and ρ_a is atmospheric

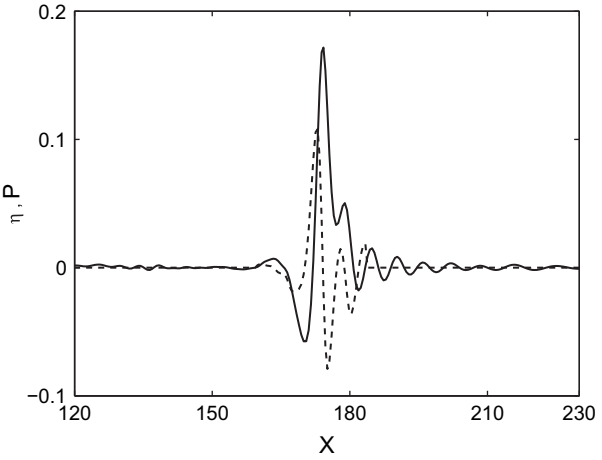

Fig. 5. Pressure at the interface (dashed line) and surface elevation (solid line) as a function of x during the occurrence of a steep wave event (η and x are given in m and $P = p_a$ in 10^{-1} Pa).

density. Kharif et al. [4] obtained an experimental value $s = 0.5$ for deep water waves. We assume that it also holds for shallow water. In order to apply the relation (18) for only steep waves we introduce a threshold value for the slope $(\partial\eta/\partial x)_c$. When the local slope of the waves becomes larger than this critical value, the pressure is given by equation (18) otherwise the pressure at the interface, p_a, is taken equal to a constant which is chosen equal to zero without loss of generality. This means that wind forcing is applied locally in time and space. When the critical value is low, the transfer of energy from the wind to the waves yields to wave breaking and when it is too high this transfer becomes negligible as far as wave dynamics are concerned. Our main purpose is to show that the application of the modified Jeffreys mechanism could explain simply some features of the interaction between wind and strongly modulated water wave groups in shallow water.

Fig. 5 shows the pressure distribution at the interface in the vicinity of the crest given by equation (18), during the occurrence of a steep wave event.

5. Numerical simulations and validation

5.1. Comparison with experiment without wind (Ricker spectrum)

To demonstrate the efficiency of the present numerical method (BIEM) used to solve the system of equations (1), (3), (4) and (5) with the boundary conditions prescribed by equation (2), a comparison between numerical results and experimental data has been done without wind.

5.1.1. Propagation of a breaking wave

The experimental simulation on the focusing phenomenon has been conducted in the wave tank of Ecole Centrale Marseille. The tank is 17 m long and 0.65 m width. The water depth in front of the wavemaker is about 0.35 m. The generation of a large wave at a given focal point follows from the focusing of waves corresponding to a given spectrum. The chosen spectrum is a Ricker spectrum (the second derivative of a Gaussian function):

$$R(\omega) = A_r\sqrt{\pi}T_r e^{-\omega^2 T_r^2/4}\left(1 - a_r\left(\frac{1}{4}\omega^2 T_r^2 - \frac{1}{2}\right)\right),$$

with A_r the amplitude of the steep wave event and a_r and T_r parameters to adjust the peak pulsation and the narrowness of the signal. A flap-type wavemaker is used to generate the focused wave. The motion of the wavemaker is calculated directly from the spectrum based on the sum of linear components as

$$\eta = \sum_{i=1}^{N} a_i \cos(k_i x - \omega_i t)$$

with the use of the linear dispersion relation $\omega_i^2 = g k_i \tan h(k_i h)$.

The spectrum is discretized with 4096 × 8 modes. The wavemaker motion is then deduced using the linear transfert function of the wavemaker.

$$C_0 = \sin h(kh)\left(\sin h(kh) + \frac{2}{k(h+l)}\,\frac{1-\cos h(kh)}{kh + \sin h(kh)\cos h(kh)}\right)$$

In this expression l corresponds to the distance from the bottom to the hinge of the wavemaker. In our case, $l = 0.5$ m corresponds to the hinge below the bottom.

Table 1
Ricker spectrum setup.

A_r (m)	a_r	T_r	Focal point (m)
0.1	−0.7	0.23	7.75

Table 2
Location of gauges.

Wave gauge n^o	1	2	3	4	5	6
Distance (m)	1.7	5.37	5.73	6.09	7	7.46

To characterize the wave field, water elevation was measured with six resistive wave gauges. The setup of the Ricker spectrum and the distance of gauges from the wavemaker are given in the following Tables 1 and 2.We run a series of numerical simulations and compare the results with experimental data. We compute exactly the wave tank of Ecole Centrale Marseille. We use a numerical flap-type wavemaker identical to the experimental wavemaker. From the experimental data, we have computed the angle of the wavemaker at every time step. To discretize the boundary the number of meshes is about 1100, 660 of them on the free surface. The time step is 10^- s. Fig. 6 shows the experimental and computed surface elevation $\eta(t)$ at $x = 1, 7$ m, $x = 5.37$ m, $x = 5.73$ m, $x = 6.09$ m, $x = 7$ m and $x = 7.46$ m. The agreement between experimental data and numerical results is satisfactory. We observe a good agreement for the phase and for the elevation despite small deviations in amplitude at $x = 1, 7$ m and phase at $x = 7.46$ m. Since we are considering near breaking and breaking waves, for which small scales are generated and surface curvature becomes important, surface tension cannot be neglected. In this experiment since we are considering a breaking wave, surface tension effect is included in the dynamical boundary condition of the fully nonlinear system. Furthermore we have introduced viscous effect. Figs. 7 and 8 show the comparisons between numerical and experimental results. The experiments correspond to dashed lines whereas solid lines correspond to numerical simulations. In Fig. 7 the numerical experiment corresponds to the case $\sigma = 0$ N m^{-1} and $\nu = 0$ m^2 s^{-1} whereas in Fig. 8 surface tension and viscous effects have been introduced ($\sigma = 73.10^{-3}$ N m^{-1} and $\nu = 10^{-6}$ m^2 s^{-1}).

As we can see the shape of the experimental and numerical breaking jets are quite similar when surface tension and viscosity are taken into account whereas it is not the case for pure gravity waves. The importance of surface tension effect is emphasized when curvature is large, namely in the vicinity of the jet. The tip of the jet is thickened in the presence of surface tension.

The number of elements has been optimized here. The number of element is sufficient since our numerical experiment fit quite well the tank experiment. Furthermore if there are too many elements this can generate singularities (small divisors) in the crest vicinity where particles accumulate during the breaking.

This comparison demonstrates the efficiency of the numerical model used to simulate realistically the formation of a steep wave event in shallow water.

5.1.2. Wall pressure exerted by a breaking wave

In this subsection we consider the pressure exerted on a vertical wall by a breaking wave in shallow water. To generate the breaking wave, the method of subsection 5.1 based on the ricker spectrum is used. We carry out a comparison with experiment too. The wave tank is 15.5 m long and the water depth h is 0.7 m. The components focus and the wave breaks just before the wall located at $x = 0$ as shown in Fig. 9. The numerical results are shown in solid line, and experimental data in dashed line. In this figure the abscissa origin is taken at the vertical wall. To discretize the boundary the number of meshes is 1000, 500 of them at the free surface, and 100 on the vertical wall. The time step is 10^{-4} s.

We compute the wall pressure $P(z)$ where z is the vertical coordinate by using the Bernoulli equation. Note that the surface

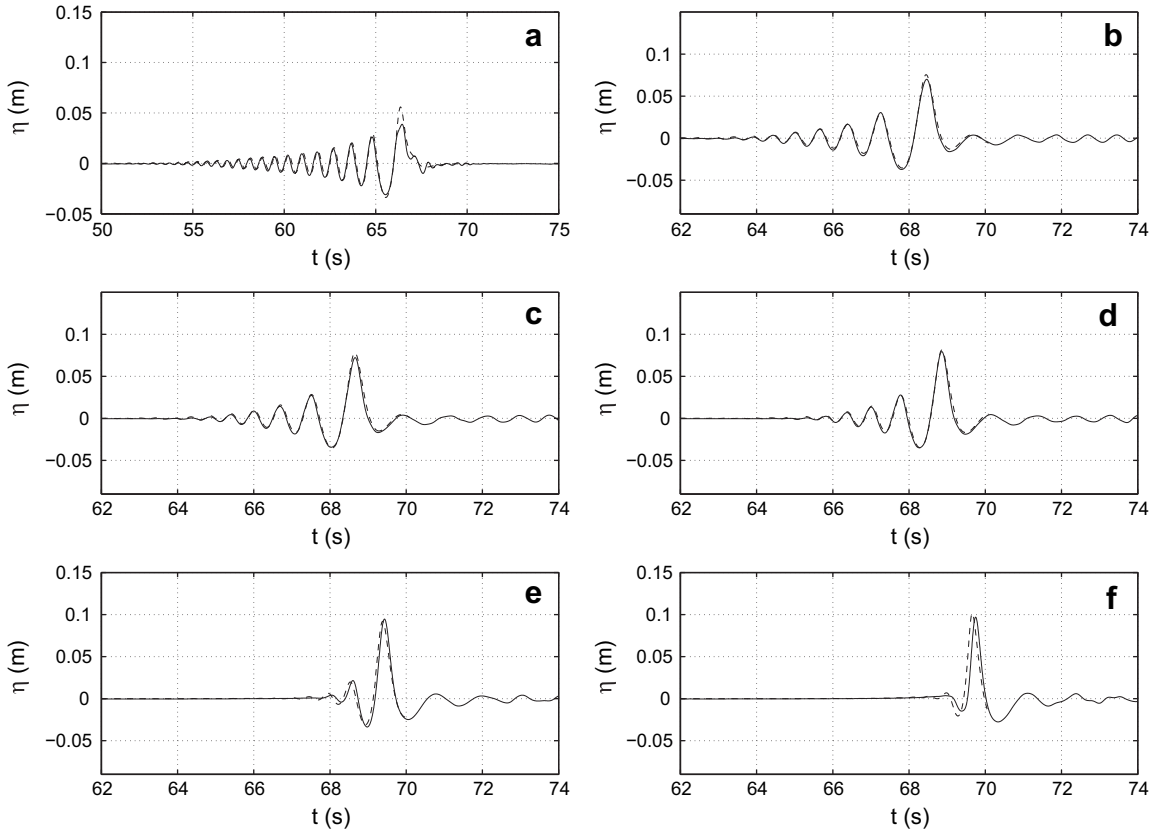

Fig. 6. Time evolution of the experimental (solid line) and numerical (dashed line) surface elevation at several fetches: (a) $x = 1$, 7 m, (b) $x = 5.37$ m, (c) $x = 5.73$ m, (d) $x = 6.09$ m, (e) $x = 7$ m and (f) $x = 7.46$ m.

tension is not neglected at the free surface. In the presence of surface tension the dynamic condition states that there is a jump of pressure at the surface due to capillary effect. However, in the present case at the point where the free surface meets the wall, the curvature radius is large enough to make the term σ/R very small.

The wall pressure is computed in the case of the breaking wave presented in Fig. 9. Fig. 10 shows the profiles of the pressure $P(z)$ at the vertical wall and the corresponding elevation of the free surface $z = \eta(x)$ at several times during the breaking. Prior to the impact of the jet on the wall (Fig. 10 right) one can observe an inversion of the vertical pressure gradient beneath the crest. This means that the vertical subsurface acceleration becomes greater than gravity. Using a PIV system Grue and Jensen [27] measured particle acceleration in overturning waves in deep water. They found that overturning events present vertical acceleration up to 1.5 g in the front face of the wave, at the base below the overturning jet. Note that in their experiments there was no wall.

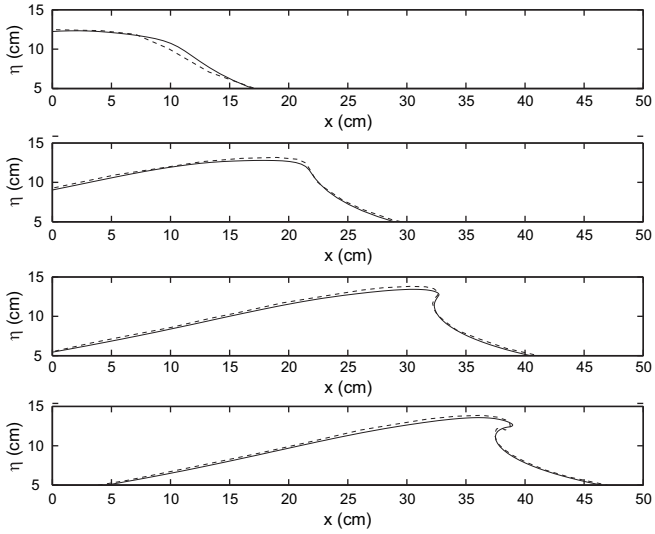

Fig. 7. Spatio-temporal evolution of a breaking wave: comparison between experimental data (dashed line) and numerical results (BIEM) without surface tension and viscosity (solid line). From top to bottom: $t = 2.19$ s, $t = 2.27$ s, $t = 2.34$ s, $t = 2.37$ s.

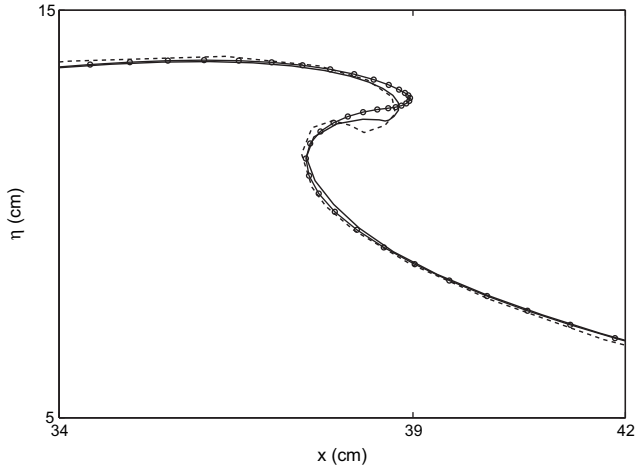

Fig. 8. Comparison between experimental data (dashed line) and numerical results (BIEM), model with surface tension and viscosity (solid line), and without surface tension and viscosity (open circles).

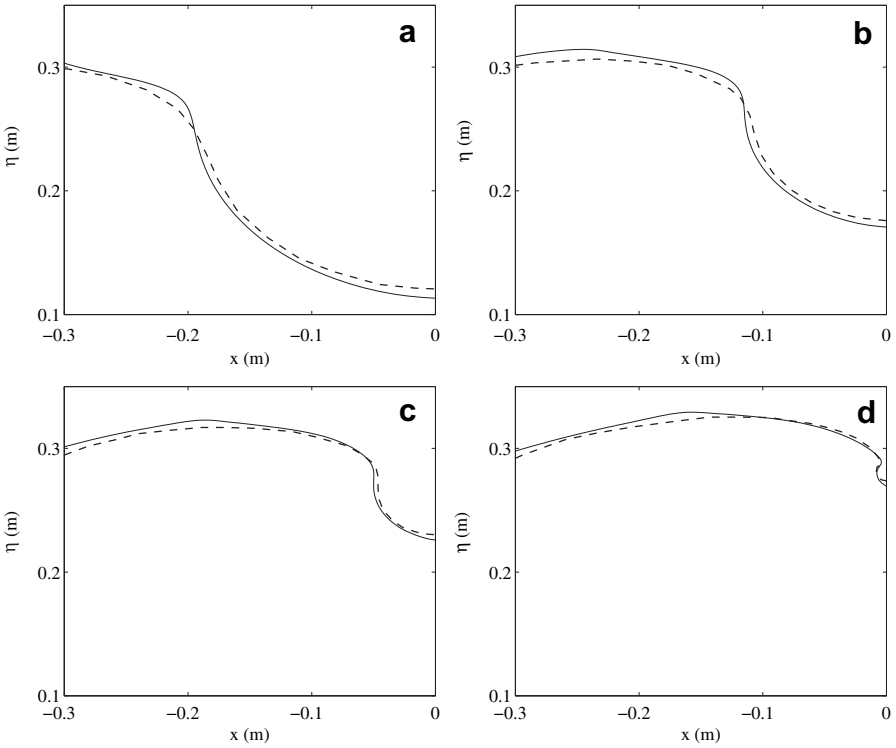

Fig. 9. Breaking wave on a vertical wall located at $x = 0$ at several times (a) $t = 2.009$ s, (b) $t = 2.0231$ s, (c) $t = 2.0394$ s, (d) $t = 2.0403$ s. Comparison with experimental data (dashed line).

The wall force due to the wave is given by

$$F_w = \int_{-h}^{\eta} P(z)\mathrm{d}z. \tag{19}$$

Fig. 11 shows the time evolution of the wall force and of the maximum pressure at the wall. At $t = 0$ s the force is mainly due to the hydrostatic pressure. At $t = 1.3$ s the wall force decreases. Indeed the arrival of a breaking wave over a wall causes a withdrawal of water at the wall and a reduction of the wetted wall surface. So during this rundown the integral of the pressure decreases. Then the runup starts at $t = 1.7$ s when the breaking wave approaches. The consequence is the increasing of the wall force. The maximum of pressure evolves in the same way that the wall force.

5.2. Steep waves under the action of wind

The question is how do steep wave events due to dispersive focusing under wind action evolve? How are the amplification and time duration of these waves under wind effect modified? Are these effects similar or different from those observed in the case of extreme wave events due to the spatio-temporal focusing in deep water?

5.2.1. Dispersive focusing

The main objective of the present subsection is to study the influence of wind on a steep wave event generated by a dispersive focusing wave train in shallow water. The wave train is generated in a numerical wave tank, and energy focusing is obtained by using the method developed in subsection 3.1. We use a piston-type

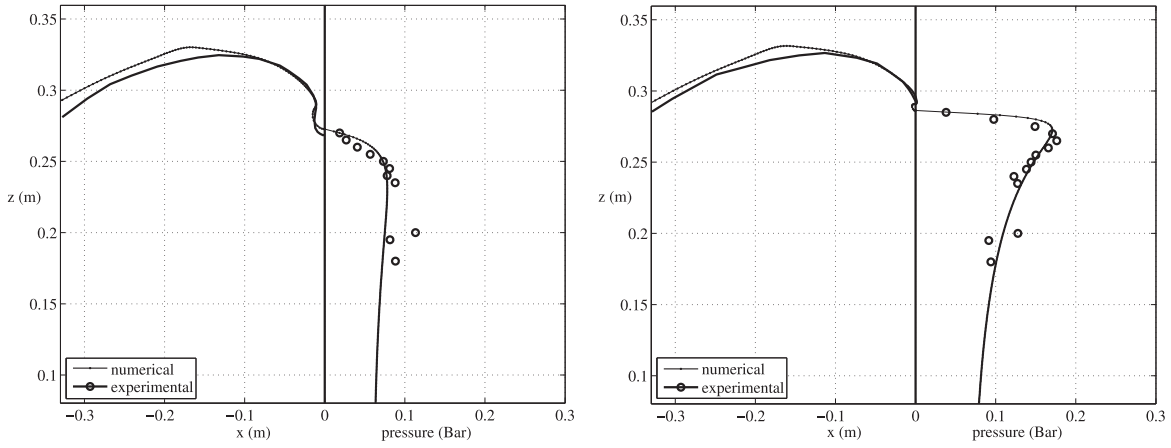

Fig. 10. Pressure at the wall during the impact. Comparison with experiment (open circles). $t = 2.05$ s (left) and $t = 2.052$ s (right).

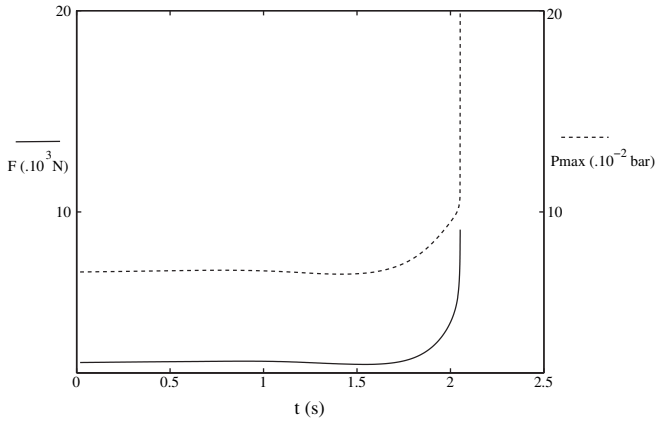

Fig. 11. Evolution of the wall force (solid line) and maximum pressure (dashed line) during the time.

wavemaker with a horizontal motion. The equation of the displacement of the wavemaker is $s(t) = A\sin(\omega(t).t)$, with $\omega(t)$ determined as in the previous subsection 3.1. The amplitude of the displacement is $A = 0.05$ m. The frequency ω is computed using the method developed in subsection 3.1 and setting $0.5 < kh < 1$. The number of meshes to discretize the boundary is 2000, 1200 of them on the water surface, and the time step is 0.05 s. The length of the tank is 400 m and depth 1 m. Fig. 12(a–d) shows the evolution of the modulated wave train in the absence of wind for different times.

The previous wave train is now submitted to the influence of wind through the modified Jeffreys' sheltering mechanism described in Section 4. The maximum value for the slope $\partial\eta/\partial x$ of the focused wave is 0.114. The threshold value for the slope $(\partial\eta/\partial x)_c$ is 0.11 and the wind velocity is $U = 20$ m s^{-1}. In Fig. 12(e–h) the influence of wind on the steep wave event is shown at the same time step than (a–d) respectively. One may observe that wind amplifies the surface elevation during the formation of steep waves.

In order to better understand the role of wind, we define the amplification factor $A(t, U)$ of the group of waves between initial time and time t as follows

$$A(t,U) = \frac{\eta_{\max}(t,U)}{\eta_{\text{ref}}}, \tag{20}$$

where η_{ref} is the maximal wave amplitude of the initial wave group. $\eta_{\max}(t, U)$ is the maximal wave amplitude of the wave group at each time.

In Fig. 13 the amplification factor as a function of time is plotted for various values of the wind velocity equal to $U = 0$ m s^{-1}, $U = 10$ m s^{-1}, $U = 20$ m s^{-1} and $U = 30$ m s^{-1}, respectively. As soon as the wave slope become greater than the threshold value we observe an amplification of the wave train. Note that a significant

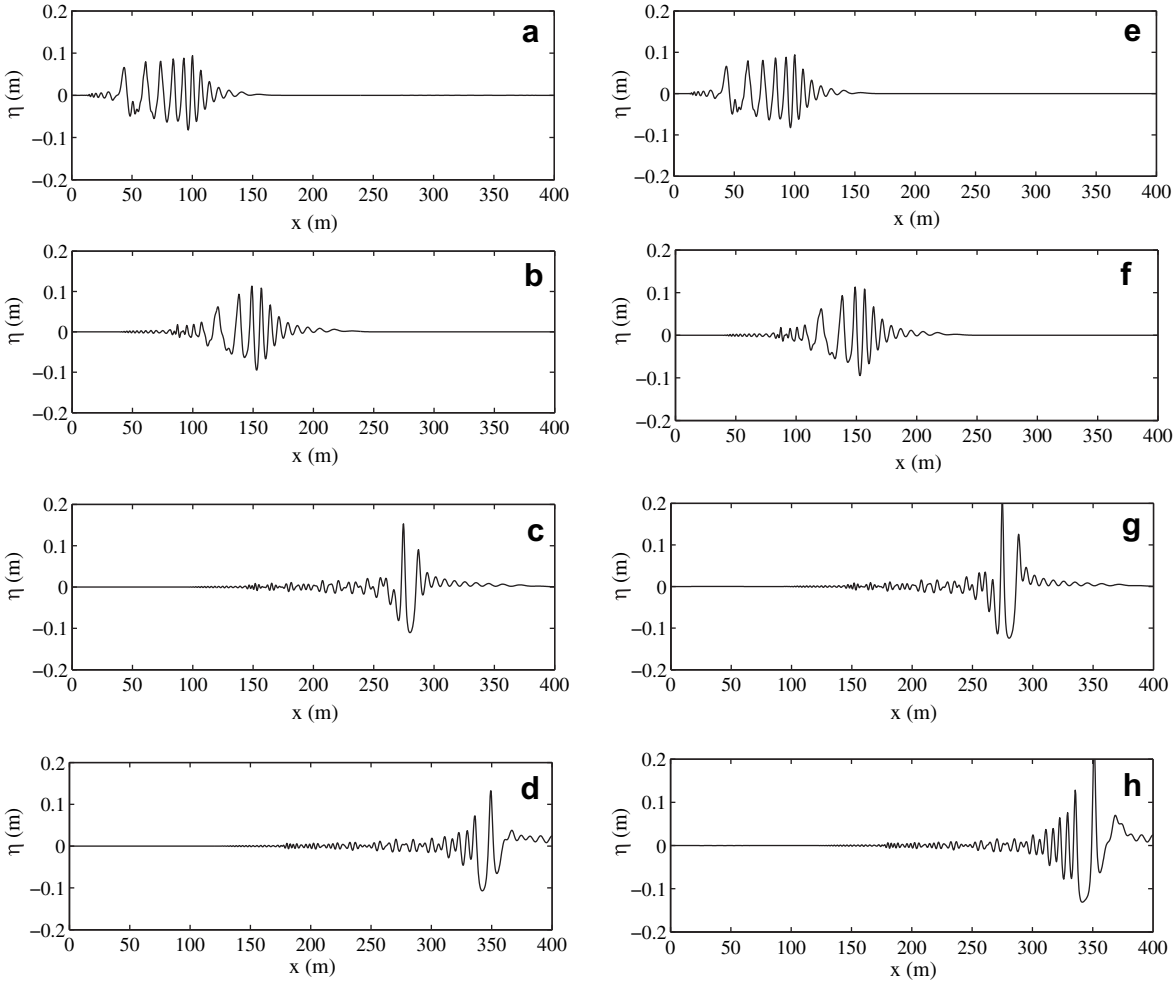

Fig. 12. Focusing wave train without wind at several times. (a): $t = 50$ s, (b): $t = 75$ s, (c): $t = 125$ s, (d): $t = 150$ s without wind, (e): $t = 50$ s, (f): $t = 75$ s, (g): $t = 125$ s, (h): $t = 150$ s with wind velocity $U = 20$ m s^{-1}.

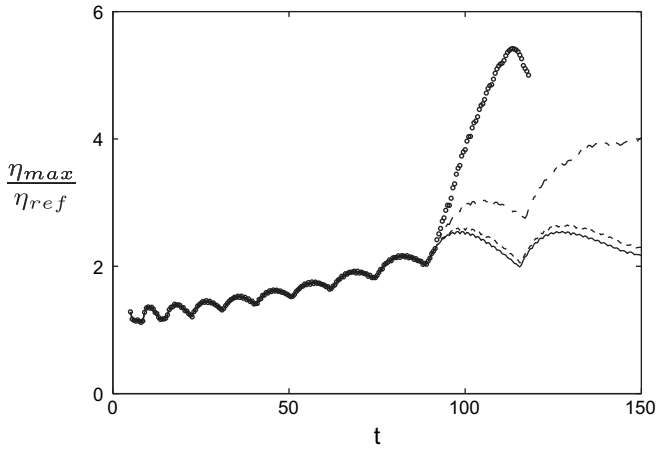

Fig. 13. Evolution of the amplification factor $A(t, U) = \eta_{max}/\eta_{ref}$ as a function of time, for several values of the wind speed (dispersive focusing). $U = 0$ m s^{-1} (solid line), $U = 10$ m s^{-1} (dashed line), $U = 20$ m s^{-1} (dot-dashed line), $U = 30$ m s^{-1} (open circle) in the dispersive focusing case.

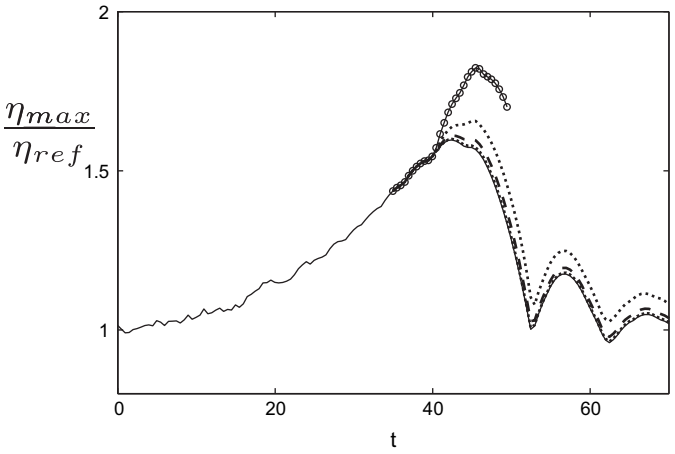

Fig. 15. Evolution of the amplification factor $A(t, U) = \eta_{max}/\eta_{ref}$ as a function of time, for several values of the wind speed (inverse method). $U = 0$ m s^{-1} (solid line), $U = 8$ m s^{-1} (dotted line), $U = 16$ m s^{-1} (dashed line), $U = 20$ m s^{-1} (dot-dashed line), $U = 30$ m s^{-1} (open circle) in the KdV inverse method case.

wind velocity is needed to influence the dynamics of the steep wave event. The amplification factor is not very different between $U = 10$ m s^{-1} and $U = 0$ m s^{-1}, i.e. without wind. For wind velocity larger than $U = 20$ m s^{-1} a significant increase of the amplification factor is obtained. The defocusing is then stopped by the breaking of the steep wave. In shallow water, strong wind velocities are needed to amplify the highest waves of the group while in deep water (see Kharif et al. [4]) lower values may increase the wave height. This feature can be explained by the fact that waves are more stable in shallow water than in deep water.

5.2.2. Korteweg de Vries equation and inverse method

We now consider the spatio-temporal evolution of the initial wave train defined in subsection 3.2 and plotted in Fig. 4. The length of the tank is 800 m and the constant water depth is 1 m. To discretize the boundary the number of meshes is 2000, 1000 of them on the free surface. The time step is 0.05 s. We show in Fig. 14 the focusing and defocusing stages of the wave train without wind effect ($U = 0$ m s^{-1}) in the plane (x, t). At the maximum of modulation the profile of the steep wave event does not fit with the expected Gaussian impulse. This discrepancy is easily explained. We have used as initial condition for the fully nonlinear system of equations (1), (3)–(5) with the boundary conditions prescribed by equation (2) the profile resulting from the KdV equation which is a weakly nonlinear model. The deviation between fully nonlinear and weakly nonlinear is due to higher-order terms which are not considered in the KdV equation.

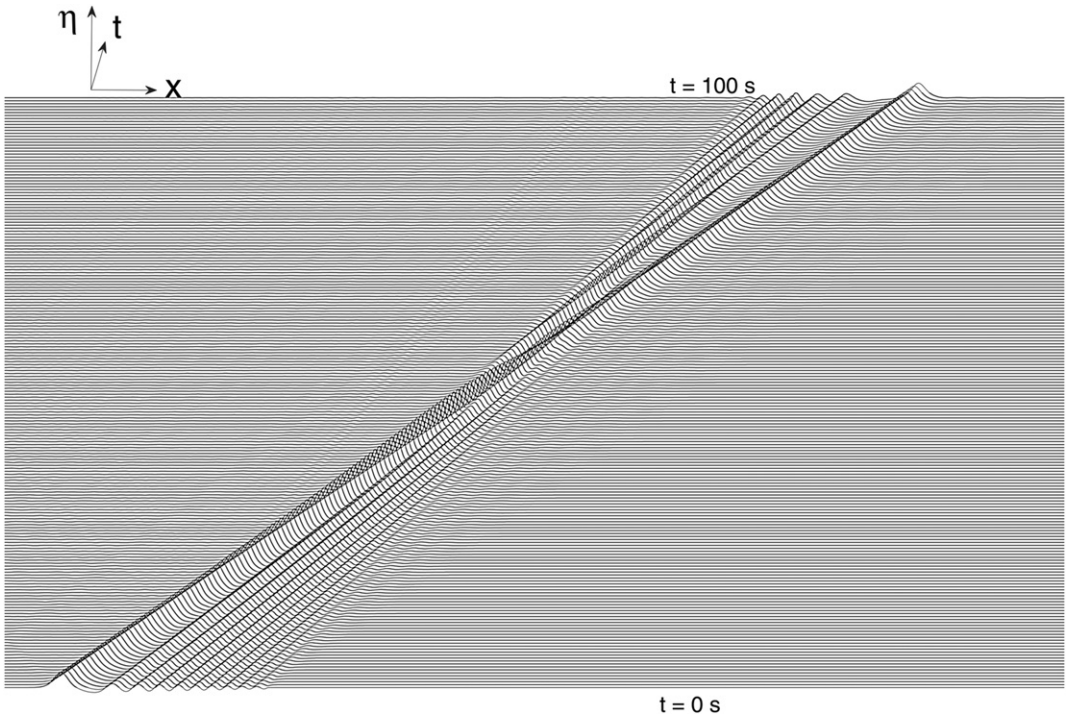

Fig. 14. Spatio-temporal evolution of the focusing and defocusing wave group in the absence of wind.

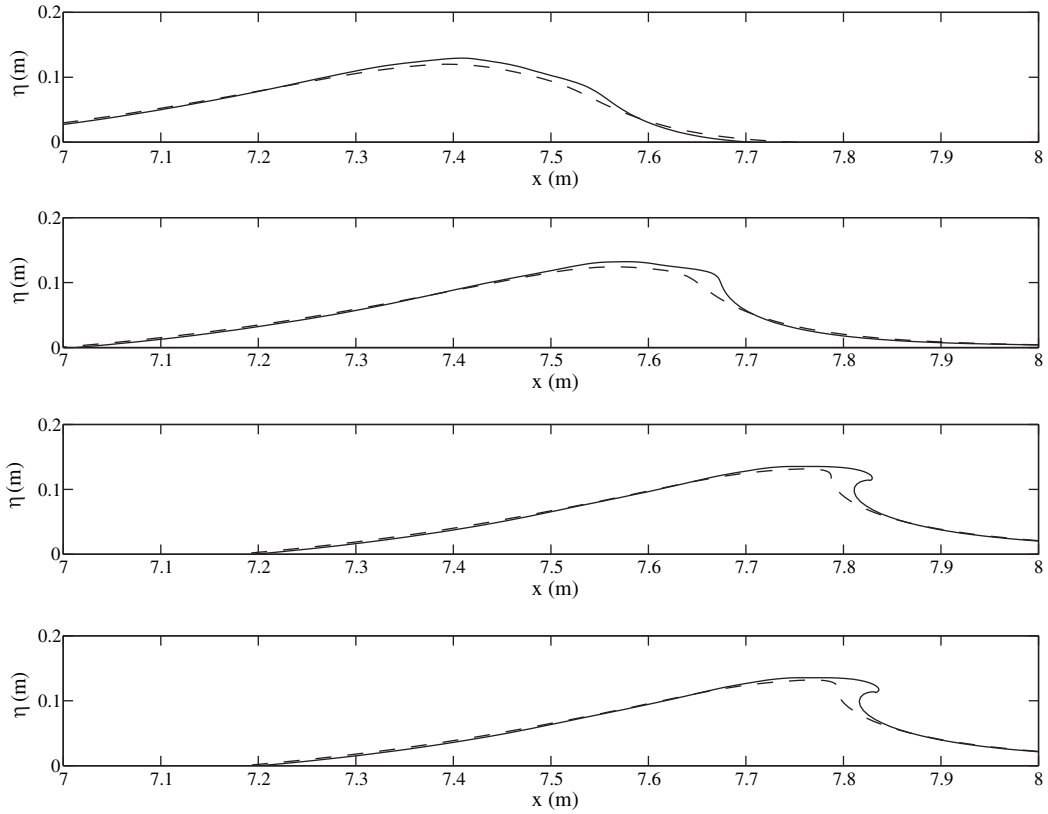

Fig. 16. Spatio-temporal evolution of breaking waves with wind (solid line) and without wind (dashed line). Wind speed is $U = 10$ m s^{-1} and critical wave slope is $\partial\eta/\partial x = 0.25$.

Fig. 15 gives the amplification factor as a function of time for various values of the wind velocity, equal to 0 m s^{-1}, 8 m s^{-1}, 16 m s^{-1}, 20 m s^{-1} and 30 m s^{-1}. The critical slope of the modified Jeffreys mechanism is $(\partial\eta/\partial x)_c = 0.20$. The maximum value for the slope $\partial\eta/\partial x$ of the focused wave is 0.24. The curves corresponding to $U = 0$ m s^{-1} and $U = 8$ m s^{-1} are almost identical. As shown in subsection 5.2.1, larger wind velocities are needed to influence the dynamics of the steep wave events. In deep water, Touboul et al. [3] and Kharif et al. [4] observed significant influence of wind on extreme wave events for weaker values of the wind speed. In relation to deep water, larger values of the wind velocity are needed in shallow water to influence significantly the behaviour of the steep wave events. This means that steep wave events are more stable to wind perturbation in shallow water than in deep water. Fig. 15 shows as well that the effect of the wind is threefold: it increases the amplification factor and lifetime of the steep wave event, and shifts downstream the focus point which corresponds to the maximum value of $A(t, U)$. For $U = 30$ m s^{-1}, the defocusing is stopped by the breaking of the wave.

5.2.3. Wind effect on breaking waves (Ricker spectrum)

In this subsection, wind effect upon the dynamics of breaking waves is investigated. We simulate numerically the spatio-temporal evolution of the wave train considered in subsection 5.1 when wind effect is introduced. The wind velocity and threshold value for the slope are $U = 10$ m s^{-1} and $(\partial\eta/\partial x)_c = 0.25$, respectively. The maximum value for the slope $\partial\eta/\partial x$ of the focused wave is 0.32. Wind effect is twofold: (i) it amplifies slightly the height of the wave and (ii) it speeds up the jet formation as shown in Fig. 16. In Fig. 17 we plot the amplification curves corresponding to three different cases. The solid line correspond to the case without wind whereas the dashed line corresponds to the case with wind. The wind speed is $U = 10$ m s^{-1} and the modified Jeffreys sheltering mechanism is applied when the wave slope satisfies the following condition: $0.25 \leq \partial\eta/\partial x \leq \tan(\pi/6)$. The value $\tan(\pi/6)$ corresponds to the Stokes corner, the limiting slope of Stokes waves. The upper bound for the wave slope has been introduced to avoid the use of equation (18) when $\partial\eta/\partial x$ becomes infinite. When the upper bound is not included, prior to breaking the wave presents a quasi vertical front with a slope close to infinity yielding to a numerical blow up. In this case the amplification factor is represented by open circles in Fig. 17. Furthermore equation (18) becomes questionable when the wave profile is multi-valued.

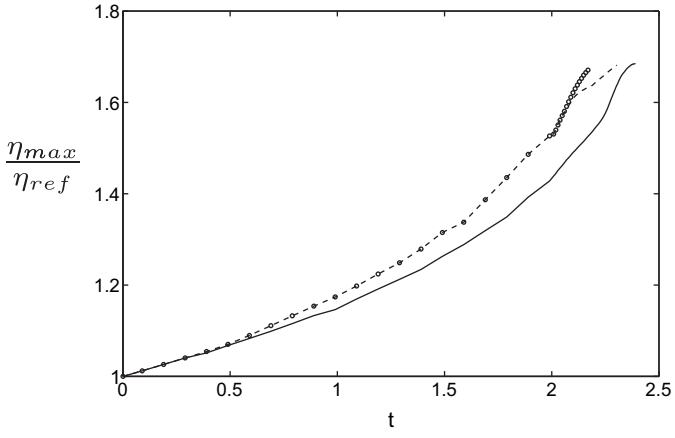

Fig. 17. Amplification factor $A(t, U) = \eta_{\max}/\eta_{\text{ref}}$ as a function of time for a focusing wave train generated from a Ricker spectrum. Without wind (solid line), with wind $U = 10$ m s^{-1}, $0.25 \leq \partial\eta/\partial x \leq \tan(\pi/6)$ (dashed line) and with wind $U = 10$ m s^{-1}, $0.25 \leq \partial\eta/\partial x$ (open circles).

6. Conclusion

One of the main objectives of this paper was to extend the results obtained by Touboul et al. [3] and Kharif et al. [4] in deep water to shallow water. The latter authors have considered the formation of steep wave events under wind action. The wind modelling is based on the Jeffreys' sheltering mechanism which is modified by introducing a threshold slope above which air flow separation can occur. In shallow water, waves are generally steep and air-flow separation is more likely to occur. We have conducted a series of numerical simulation of steep wave events in shallow water. We used a dispersive focusing mechanism and an inverse method to generate steep wave groups. We found that focused steep gravity waves behaves similarly in shallow water and deep water. The main effect of wind is threefold: (i) it increases the amplitude and lifetime of the highest waves in the group and (ii) it moves downwind the area where steep wave events are formed. In addition, we observed that the steep wave events are less unstable to wind perturbation in shallow water than in deep water. In other words, stronger wind are required in finite depth to produce breaking waves.

To compare with experiments on plunging breaker on a vertical wall conducted in the wave tank of Ecole Centrale Marseille, a series of numerical simulation has been performed. The breaking wave is obtained by focusing wave energy from a Ricker spectrum. The role of surface tension effects has been emphasized to describe accurately the profile of the breaking jet. Wind effect has been introduced and it was found that it speeds up the overturning of the crest. During the formation of the breaking wave the pressure is no more hydrostatic and an inversion of the vertical pressure gradient is observed beneath the water surface.

References

[1] C. Kharif, E. Pelinovsky, A. Slunyaev, Rogue Waves in the Ocean. Springer-Verlag, Berlin Heidelberg, 2009.
[2] M.L. Banner, J. Song, On determining the onset and strength of breaking for deep water waves. Part II: influence of wind forcing and surface shear. J. Phys. Oceanogr. 32 (2002) 2559–2570.
[3] J. Touboul, J.P. Giovanangeli, C. Kharif, E. Pelinovsky, Freak waves under the action of wind: experiments and simulations. Eur. J. Mech. B Fluids 25 (2006) 662–676.
[4] C. Kharif, J.P. Giovanangeli, J. Touboul, L. Grare, E. Pelinovsky, Influence of wind on extreme wave events: experimental and numerical approaches. J. Fluid Mech. 594 (2008) 209–247.
[5] Q.W. Ma, S. Yan, Preliminary Simulation on Wind Effects on 3D Freak Waves. Rogue Wave, Brest, France, 2008.
[6] Yan S, Ma QW. Numerical simulation of wind effects on breaking solitary waves. In: 19th Int. Offshore and Polar Eng. Conf., (Osaka, Japan) 2009. p. 480–7.
[7] Chambarel J, Kharif C, Kimmoun O. Focusing wave group in shallow water in the presence of wind, discrete and continuous dynamical systems – series S, AIMS' Journal, in press.
[8] H. Oumeraci, Review and analysis of vertical breakwater failures â″ lessons learned. Coast. Eng. 22 (1994) 3–29.
[9] E.S. Chan, W.K. Melville, Deep water plunging-wave pressures on a vertical plane wall. Proc. R. Soc. London 417 (1988) 95–131.
[10] M.S. Kirkgöz, An experimental investigation of a vertical wall response to breaking wave impact. Ocean. Eng. 17 (1990) 379–391.
[11] M.S. Kirkgöz, Impact pressure of breaking waves on vertical and sloping walls. Ocean Eng. 18 (1991) 45–59.
[12] M. Hattori, A. Arami, T. Yui, Impact wave pressure on vertical walls under breaking waves of various types. Coast. Eng. 22 (1994) 79–114.
[13] G.N. Bullock, C. Obhrai, D.H. Peregrine, H. Bredmose, Violent breaking wave impacts. Part 1: results from large-scale regular wave tests on vertical and sloping walls. Coast. Eng. 54 (2007) 602–617.
[14] M.J. Cooker, D.H. Peregrine, Wave impact pressure and its effect upon bodies lying on the bed. Coast. Eng. 18 (1992) 205–229.
[15] D.H. Peregrine, Water-wave impact on walls. Annu. Rev. Fluid Mech. 35 (2003) 23–43.
[16] Cooker MJ, Peregrine DH. A model for breaking wave impact pressures. In: Proc. 22nd Int. Conf. Coast. Eng., 2; 1990, 1473–86.
[17] S. Zhang, D.K.P. Yue, K. Tanizawa, Simulation of plunging wave impact on a vertical wall. J. Fluid Mech. 327 (1996) 221–254.
[18] D. Ruvinsky, T.F.I. Feldstein, G.I. Freidman, Numerical simulations of the quasi-stationary stage of ripple excitation by steep gravity-capillary waves. J. Fluid Mech. 230 (1991) 339–353.
[19] G.B. Whitham, Linear and Nonlinear Waves. Wiley, 1974.
[20] L. Ostrovsky, A. Potapov, Modulated Waves, Theory and Applications. John Hopkins University Press, Baltimore, 1999.
[21] M.G. Brown, Space-time surface gravity waves caustics: structurally stable extreme events. Wave Motion 33 (2001) 117–143.
[22] E. Pelinovsky, T. Talipova, C. Kharif, Nonlinear dispersive mechanism of the freak wave formation in shallow water. Phys. D 147 (2000) 83–94.
[23] B. Fornberg, A Practical Guide to Pseudo-Spectral Methods. Cambridge University Press, 1998.
[24] H. Jeffreys, On the formation of wave by wind. Proc. R. Soc. Lond. A 107 (1925) 189–206.
[25] M.L. Banner, W.K. Melville, On the separation of air flow over water waves. J. Fluid Mech. 77 (1976) 825–842.
[26] S. Kawai, Structure of air flow separation over wind wave crests. Boundary-Layer Meteorol. 23 (1982) 503–521.
[27] J. Grue, A. Jensen, Experimental velocities and accelerations in very steep wave events in deep water. Eur. J. Mech. B Fluids 25 (2006) 554–564.